ACS APPLIED ENERGY MATERIALS

www.acsaem.org
Article

Pyridinium-Benzoxazole-Based Anode Material for Sustainable All-Organic Polymer-Based Batteries

Xhesilda Fataj, Andreas J. Achazi, Christian Stolze, Simon Muench, René Burges, Ilya Anufriev, Manon Mignon, Doreen Mollenhauer, Ivo Nischang, Martin D. Hager, and Ulrich S. Schubert*

Cite This: ACS Appl. Energy Mater. 2025, 8, 4220−4230
Read Online

ACCESS | Metrics & More | Article Recommendations | Supporting Information

ABSTRACT: In search of anode materials for organic batteries, we propose benzoxazole-based redox-active polymers. We report theoretically calculated redox properties of the monomer and polymer based on small polymer chain models using density functional theory (DFT). Subsequently, a straightforward synthesis of poly(4-(benzoxazol-2-yl)-1-(4-vinyl benzyl)pyridinium chloride) (PBO) via radical polymerization is presented. To our knowledge, PBO is the first representative of this class of redox-active polymers applied in batteries, and it has a theoretical specific capacity of 76.8 mA h g^{-1} (first redox process). PBO was utilized as an anode and capacity-limiting electrode in an all-organic radical battery using aqueous- and organic-based electrolytes as well as 2,2,6,6-tetramethylpiperidinyl-*N*-oxy (TEMPO) derivatives as cathodes, providing a cell voltage of 1.3 and 1.4 V in aqueous- and organic-based electrolytes, respectively. The material revealed 99% capacity utilization at 1 C in the first cycle using an organic electrolyte (1 M $LiClO_4$ in CH_3CN) and more than 75% capacity utilization in an aqueous electrolyte (1 M $LiClO_4$ in H_2O). In both systems, after rate capability tests (from 0.2 to 50 C), the cells were cycled again at 1 C, where 50% of the initial capacity was retained after 100 cycles. Even though, due to the linearity and the molar mass of PBO, a capacity decay is observed during cycling tests, this study opens a promising class of molecules for the development of anode materials.

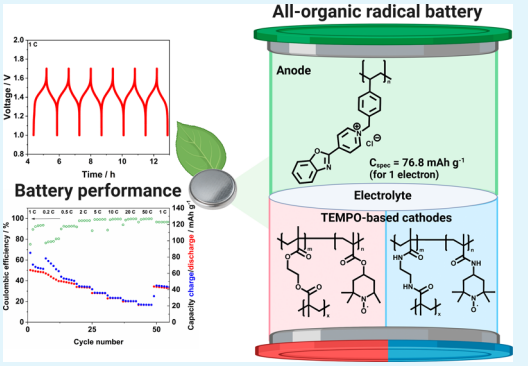

KEYWORDS: *polymer battery, organic battery, poly(benzoxazole), anode material, TEMPO derivatives*

1. INTRODUCTION

Technologies for sustainable energy storage have received increasing attention over the past decade. One of the most promising energy storage technologies is batteries. Currently, Li-ion batteries are mainly used due to their high energy density and long cycle life. Still, one of the drawbacks of this technology is its reliance on metal oxide-based materials such as nickel and cobalt oxides.[1] However, there is a more sustainable battery chemistry technology thriving, which is based on redox-active organic compounds.[1−3] Organic and polymeric active materials have been introduced in small-molecule batteries,[4] redox-flow batteries,[5] organic/metal batteries (e.g., Li, Na, Mg, and Zn), also known as semiorganic batteries,[7−10] and all-organic batteries.[11−13]

A number of organic cathode materials have been reported and studied in semiorganic batteries.[14] Here, one can mention molecules such as 2,2,6,6-tetramethylpiperidinyl-*N*-oxy (TEMPO) introduced to the battery research by the Nishide group in the early 2000s,[6,7,15−17] phenothiazine-based active molecules, e.g., poly(vinylphenothiazine),[18] and quinone-based molecules, e.g., poly(benzoquinonyl sulfide).[19] More examples can be found in the publication of Poizot et al.[14] Regarding anode materials, there is still much research to be performed.[1,14] One of the most often applied anode materials in all-organic polymer-based batteries is pyridine-based molecules, in particular, molecules which rely on 4,4′-bipyridine units (i.e., viologen) within the main or side chain of the polymer. Viologen-based materials have been proven to be compatible with both aqueous and organic electrolytes but often require elaborate synthetic routes, and their stability is still an issue of ongoing investigations.[20−22] This highlights the demand for additional molecules to be investigated, which can compete with the performance of viologen but are synthetically easier to access and more stable.[23−25]

When exploring new polymer materials for integration into organic batteries, computational methods and molecular modeling offer a valuable contribution to understand and to screen the electrochemical properties of organic active material.[24,26−29] Additionally, while designing a new organic active material, several aspects must be considered. These include prioritizing a straightforward as well as cost-effective

Received: December 5, 2024
Revised: February 13, 2025
Accepted: February 19, 2025
Published: March 20, 2025

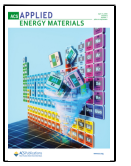

synthetic process and, most importantly, a crucial focus on the material's sustainability. In our previous research, we investigated the electrochemical properties of benzothiazoles, oxazoles, and imidazoles, both theoretically and experimentally. The benzoxazole excelled among the investigated molecules with two reversible redox processes at −1.1 and −1.85 V vs $Ag/AgNO_3$ reference electrode.[24]

This study focuses on an all-organic polymer thin-film battery based on benzoxazoles (BOs). Prior to synthesis, theoretical calculations of the redox potentials of 4-(benzoxazol-2-yl)-1-(4-vinyl benzyl)pyridinium (BO monomer) and a small polymer unit of poly(4-(benzoxazol-2-yl)-1-(4-vinyl benzyl)pyridinium chloride) (PBO) were performed by using density functional theory (DFT). The aim was to estimate the reduction and oxidation potentials of the redox-active molecules and to investigate the influence of side-chain interactions on these redox potentials. For practical tests, the PBO linear polymer was synthesized by the radical polymerization of the styrene-based benzoxazole monomer. In the end, an all-organic-polymer battery using PBO as anode material providing a specific capacity of 154 mA h g^{-1} (two redox processes) vs well-known TEMPO derivatives was prepared. For a better understanding of the anode material, several electrolyte systems (organic- and aqueous-based) commonly applied in organic batteries were investigated.[30,31] For each system, a counter electrode that works best in an organic or aqueous environment was used. More specifically, poly(TEMPO-methacrylate) (PTMA) and poly(TEMPO-methacrylamide) (PTMAm) with specific capacities of 112 and 111 mA h g^{-1} were employed, respectively (Scheme 1). Further information on the polymer synthesis of PTMA and PTMAm can be found in literature.[7,16] These batteries combining PTMA or PTMAm as a positive and PBO as a negative electrode result in a full-organic cell type operating in an anion rocking chair configuration, where only the anion is used as a charge carrier. These batteries can be engineered to operate without metal ions, further enhancing their sustainability.[32−36] The development of sustainable and high-performance energy storage systems is crucial for the advancement of renewable energy technologies. We believe that the investigation of the PBO redox-active polymer, from theoretical calculations to synthesis and characterization to implementation as an anode material, will contribute to the development of new redox-active materials used in ecofriendly energy storage solutions.

2. RESULTS AND DISCUSSION

2.1. Monomer and Polymer Synthesis. Two linear cationic polymers named poly(4-(benzoxazol-2-yl)-1-(4-vinyl benzyl)pyridinium chloride) (PBO) with different molar masses were synthesized: **P1-PBO** and **P2-PBO**. The synthetic procedure was as follows. The monomer 4-(benzoxazol-2-yl)-1-(4-vinyl benzyl)pyridinium chloride (BO monomer) was obtained by reaction of 2-(pyridine-4-yl)benzoxazole synthesized as in our previous work with commercially available 4-vinylbenzylchloride at 50 °C for 19 h (Scheme 2).[24] The obtained monomer was used for free radical polymerization using 5 mol % 4,4-azo-bis(4-cyanovaleric acid) (ACVA) in a water−dioxane mixture. For **P1-PBO**, the polymerization was performed at 100 °C for 4 h, and for **P2-PBO**, at 85 °C for 6 h. The lower temperature results in longer chain formation, i.e., a higher molar mass. Apparent molar masses were estimated by sedimentation velocity analytical ultracentrifugation (SV AUC) experiments in methanol. The analysis of SV AUC experiments

Scheme 1. Schematic Representation of the Organic Battery System Being Investigated Here[a]

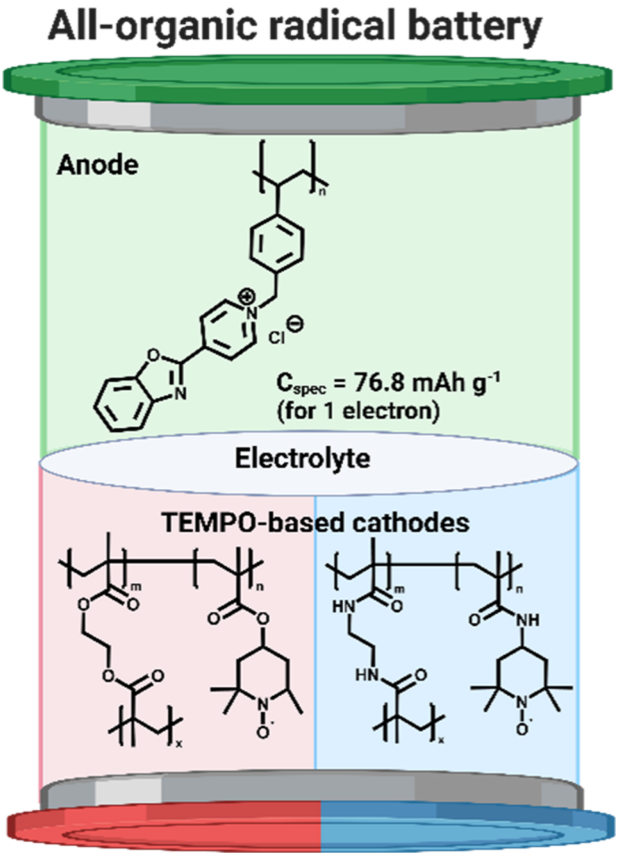

[a]PBO as anode material and TEMPO derivatives as cathode interacting with aqueous- and organic-based electrolytes.

by numerical solution of the Lamm equation via the $c(s,f/f_0)$ model resulted in differential distributions of sedimentation coefficients (normalized differential distributions of sedimentation coefficients of **P1-PBO** and **P2-PBO** are shown in Figure S5).[37,38] The distributions indicate readily disperse polymer populations in solution.[38] Signal (weight) average sedimentation coefficients, s, were obtained by integration over the whole range of sedimentation coefficients. The obtained translational frictional ratios, f/f_{sph}, from sedimentation−diffusion analysis then enabled the calculation of the molar masses by the modified Svedberg equation ($M_{s,f}$) (eq S1). The molar mass values, calculated by eq S1, are $M_{s,f}$ = 3500 g mol^{-1} for **P1-PBO** and $M_{s,f}$ = 5100 g mol^{-1} for **P2-PBO**. The determined hydrodynamic characteristics of the studied polymers are reported in Table S1 of the Supporting Information. We note that molar mass estimations using this approach can be prone to error due to the readily high dispersity of the polymer populations. A further detailed discussion on SV AUC data and properties of studied polymers can be found in the Supporting Information, alongside characterization to confirm the chemistry, structure, and purity of the small molecule, monomer, and polymer (^1H and ^{13}C NMR, elemental analysis, and high-performance liquid chromatography (HPLC) characterizations can be found in the Supporting Information).

2.2. Theoretical Calculations. DFT calculations were performed to determine the reduction/oxidation potentials of the monomer and different polymer model systems. For this

https://doi.org/10.1021/acsaem.4c03127
ACS Appl. Energy Mater. 2025, 8, 4220−4230

Scheme 2. Schematic Representation of the Synthesis of the Monomer and the Linear Oxazole-Based Polymers, P1-PBO and P2-PBO

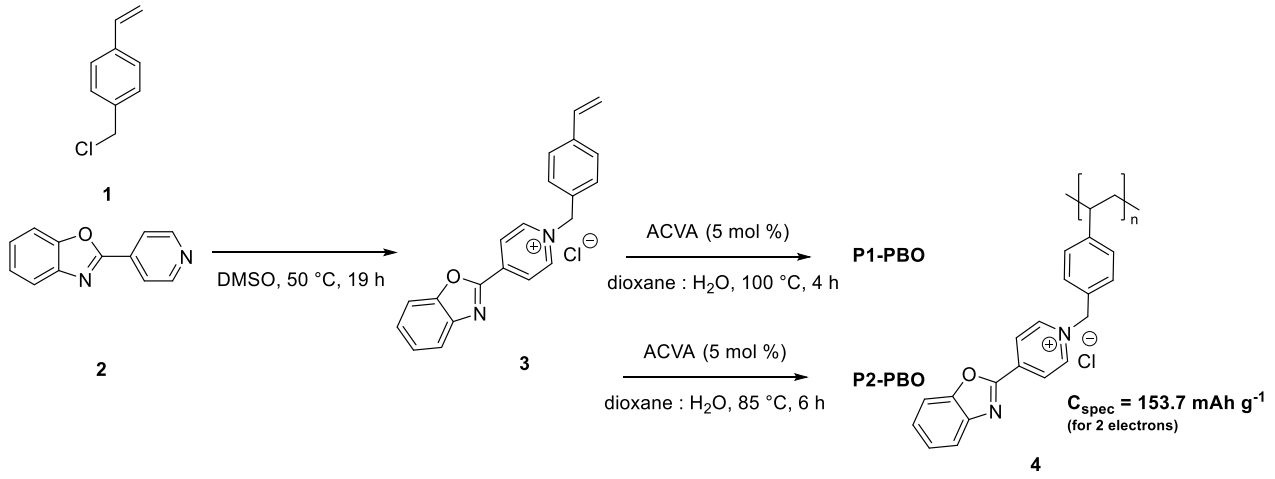

purpose, trimer (BO trimer) chains as well as pentamers (BO pentamer, see Supporting Information) of 4-(benzoxazol-2-yl)-1-(4-vinyl benzyl)pyridinium (BO) were utilized as model systems for PBO. The theoretical investigation of the trimer and pentamer model systems with multiple unpaired electrons required a hybrid density functional. Based on our method validation for calculating the reduction/oxidation potentials of the corresponding BO monomer in our previous study,[26] the B3LYP-D4/def2-TZVP[39−48] (COSMO) level of theory was chosen for the theoretical consideration. In what follows, the calculated oxidation potential E^0_{Ox} here refers to the potential required to oxidize the neutral species to the cationic species, which is related to the half-wave potential obtained during the first oxidation/reduction process in the experimental CVs (it is referred to as $E_{1/2}$ oxidation in Table 1). The calculated reduction potential E^0_{Red} refers to the potential needed to reduce the neutral species to the anionic species, which is related to the half-wave potential obtained during the second reduction/oxidation process in the experimental CVs (it is referred to as $E_{1/2}$ reduction in Table 1). The calculated oxidation potentials E^0_{Ox} and reduction potentials E^0_{Red} for the BO monomer and BO trimer are given in Table 1 together with the corresponding experimental results. The calculated oxidation potential for the BO monomer differs by only −0.05 V from the experimental value. For the reduction potential, the deviation is −0.22 V. Our previous method evaluation[26] and study[24] revealed that the deviations are mainly constant shifts and that trends in redox potentials are reproduced well.

Table 1. Reduction and Oxidation Potentials Experimentally Obtained vs the Theoretical Calculated Reduction/Oxidation Potentials E^0_{Red} and E^0_{Ox} at the B3LYP-D4/def2-TZVP (COSMO-Outer Charge: CH_3CN) Level of Theory[a]

	$E_{1/2}$ reduction vs $Ag/AgNO_3$ in V	$E_{1/2}$ oxidation vs $Ag/AgNO_3$ in V
BO monomer	−1.83	−1.05
PBO	−1.81	−1.03
	E^0_{Red} vs $Ag/AgNO_3$ in V	E^0_{Ox} vs $Ag/AgNO_3$ in V
BO monomer	−2.05	−1.10
BO trimer, one (or two) BO unit(s) reduced/oxidized	−2.06 (−2.19)	−1.26 (−1.05)

[a]The thermal contributions are calculated with the same method but the def2-SVP basis set. The BO trimer with one or two oxidized/reduced BO units is used as a model system to estimate the redox properties of PBO.

The experimental results show that the first reduction/oxidation half-wave potential of PBO differs by 0.02 V from the BO monomer. The calculated oxidation potential of the BO trimer with one oxidized BO unit is 0.16 V lower, and with two oxidized BO units, it is 0.05 V higher compared to the calculated BO monomer. This difference is in reasonable agreement with the difference between the experimental values for the monomer and polymer, taking into account the accuracy of the DFT method applied.[26] To understand the BO trimer model in more detail, the spin and charge distributions are taken into account (Figure 1). In the neutral species of the BO trimer, the three unpaired electrons are equally localized over the π-systems (Figure 1a). In the cationic trimer (Figure 1c), the spin density on one of the outer BO units almost does not change, while the central BO unit and the other outer BO unit lose the same amount of spin density. This indicates that one unpaired electron is on the outermost BO unit, and the other is equally delocalized over the central and other outermost BO unit. Hence, the positive charge is also delocalized over the central and one outermost BO unit, see, e.g., the electrostatic potential map (EMP) of the cationic BO trimer (Figure 1d). It shows a strongly positive surface (dark blue) at the pyridyl units of the central and one outermost BO unit. The delocalization is associated with a reduced distance (Table S4, distances between C2 atoms in the BO units, Supporting Information) between the BO units in the cationic species. Interestingly, the charge and spin density of the model system with two BO units oxidized are located on individual BO units (outer units) in the BO trimer (structures of the BO trimer in various charge states can be found in the Supporting Information, Figure S6). This makes the oxidation less favorable and more similar to the oxidation of a BO monomer. In addition, the oxidation of two BO units is slightly less favorable because of the electrostatic repulsion between the two charged centers. Furthermore, the results suggest that the electrochemical reactions take place first in BO units that are far apart and last in adjacent BO units.

https://doi.org/10.1021/acsaem.4c03127
ACS Appl. Energy Mater. 2025, 8, 4220−4230

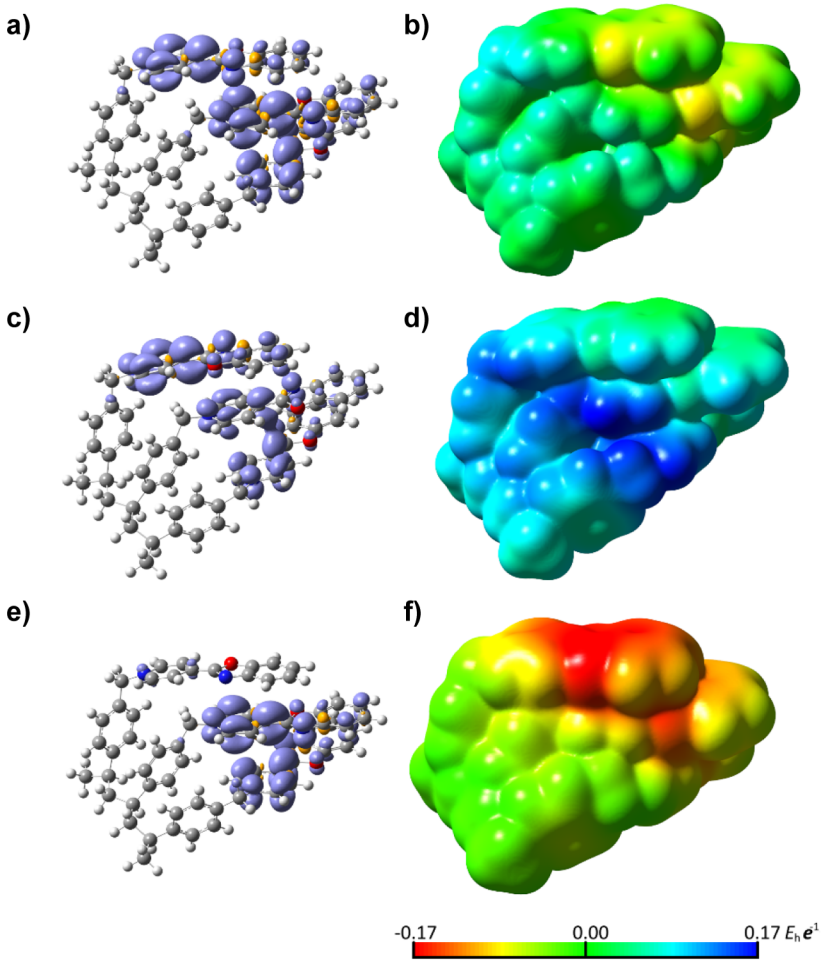

Figure 1. (a,b) Spin density and EMP of the neutral BO trimer; (c,d) spin density and EMP of the cationic BO trimer; (e,f) spin density and EMP of the anionic BO trimer. Gray: carbon. Blue: nitrogen. Red: oxygen. White: hydrogen. Purple and orange: α spin density minus β spin density.

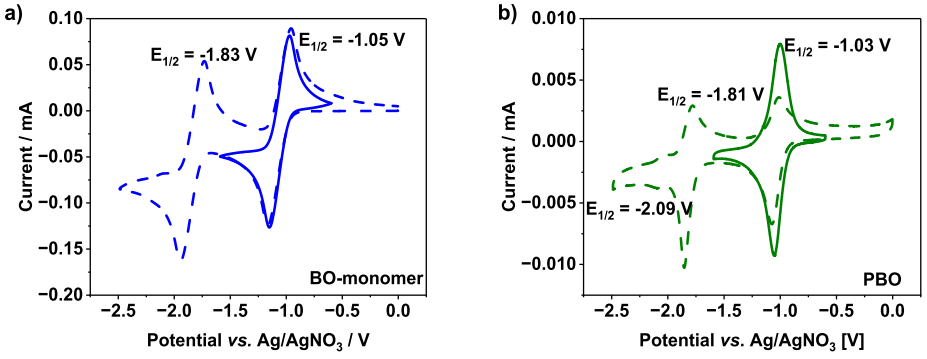

Figure 2. Cyclic voltammetry curves in solutions of (a) BO monomer and (b) PBO polymeric active material in a three-electrode setup using 0.1 M TBAPF$_6$ in CH$_3$CN. The results indicated two distinct redox processes, as shown by the dashed line on the graph. The first redox process (which is also emphasized by the full line) occurred at $E_{1/2\ \text{oxidation}} = -1.05$ V for the monomer and $E_{1/2\ \text{oxidation}} = -1.03$ V for PBO, while the second occurred at $E_{1/2\ \text{reduction}} = -1.83$ V for the monomer and $E_{1/2\ \text{reduction}} = -1.05$ V vs Ag/AgNO$_3$ for PBO.

The experimental results show that the second reduction/oxidation half-wave potential of PBO also differs by 0.02 V from that of the BO monomer. This difference is in good agreement with the difference between the calculated reduction potential of the BO monomer and the reduction potential of the BO trimer with one reduced BO unit, indicating good agreement between computational values and experiment. The reason for the similarity between the monomer and trimer is that for the anion, the charge is not delocalized across the BO units. Instead, the additional electron and negative charge (Figure 1e,f) are mainly localized at one of the outer BO units. The distances between the BO units in the anionic species (Table S4, Supporting Information) also remain similar to the distances in the neutral species. However, the reduction potential for two BO units reduced in the BO trimer is more negative (by 0.14 V) than that for the BO monomer. This is probably due to the additional electrostatic repulsion between the two charged BO

https://doi.org/10.1021/acsaem.4c03127
ACS Appl. Energy Mater. 2025, 8, 4220−4230

Scheme 3. Schematic Representation of the Structure of Linear PBO, PTMA, PTMAm, and Their Redox Processes

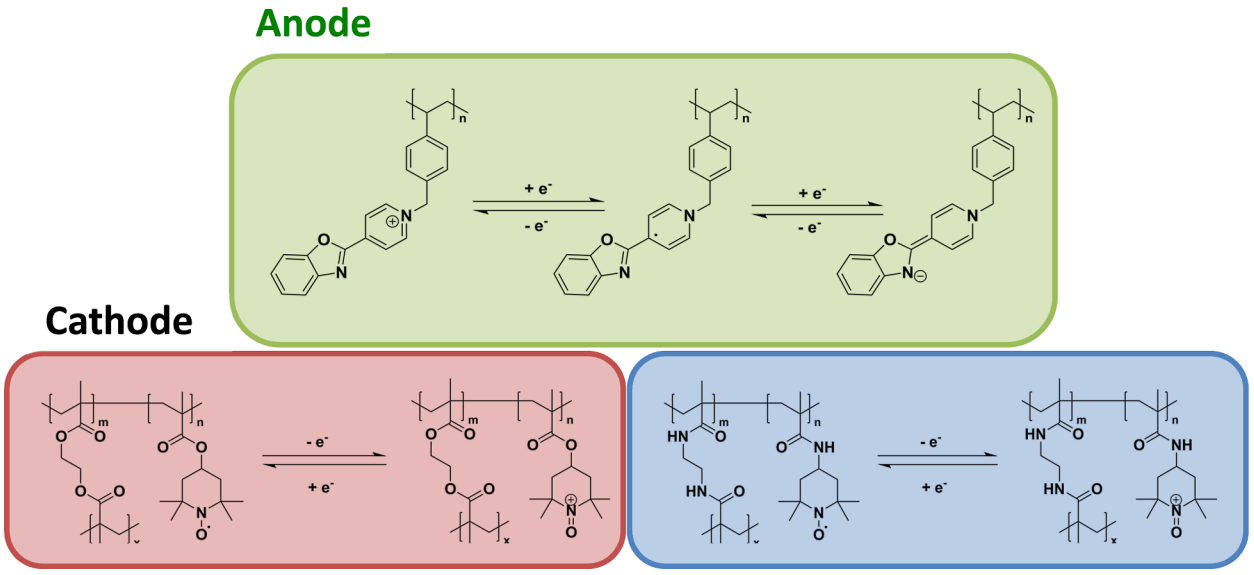

units in the doubly charged anion. The charges and spin densities are also localized at individual BO units (outer units) in the BO trimer (structures of the BO trimer in various charge states, Figure S6). This also suggests that the electrochemical reactions take place first in BO units that are far apart and last in adjacent BO units.

Overall, the calculated results reveal promising redox properties. The calculations for the polymer model systems predict that the redox potentials of PBO are similar to or lower than those of the BO monomer. Furthermore, the results suggest that the side chains exert a greater influence on the oxidation potential than on the reduction potential. However, the deviations between the oxidation and reduction potentials of one and two BO units may be due to explicit solvent and counterion effects. Our previous study indicated that in certain cases counterions probably have an effect on the reduction/oxidation potential.[24] The inclusion of counterion effects may potentially reduce electrostatic repulsion between the charged centers and by this make the redox potential more similar to the ones found for the BO monomer.

2.3. Electrochemical Investigation. Before the electrochemical performance of the obtained polymer in a battery was investigated, cyclic voltammetry (CV) in solution was performed on the BO monomer (Figure 2a) and PBO (Figure 2b). As mentioned previously, both the benzoxazole-based monomer and PBO reveal two distinct redox processes: the monomer at $E_{1/2\ \text{oxidation}} = -1.05$ and $E_{1/2\ \text{reduction}} = -1.83$ V and PBO at $E_{1/2\ \text{oxidation}} = -1.03$ and $E_{1/2\ \text{reduction}} = -1.81$ V vs $Ag/AgNO_3$ (0.1 M $TBAPF_6$ in CH_3CN) reference electrode. These processes involve the reduction of the monovalent cation to the radical and further to the monovalent anion (Scheme 3). Previous investigations of PTMAm and PTMA result in half-wave potentials of 0.64 vs Ag/AgCl[49] and 0.84 V vs Ag/Ag^+,[16] respectively. Both TEMPO-based polymers are oxidized from their neutral radical to form a monovalent cation (Scheme 3).

An additional small redox event appears at lower potentials (Figure 2b). It is possible that a side reaction occurs during the reduction or oxidation of the system. The sharp reduction peak and the different peak heights indicate further that the redox event is complicated by other processes when compared to the small molecule (Figure 2a). During our previous investigations,[24] we identified the first reduction/oxidation process to be more stable within different scanning rates, and thus, for the present study, only the first reversible reduction/oxidation process was covered during the battery experiments in order to prevent possible side reactions. When assembling the full organic battery, a voltage window of 1.0 to 1.7 V was applied, resulting in defined redox processes with a battery voltage of 1.3 V for the aqueous system and 1.4 V for the organic system vs the respective TEMPO-based counter electrode without the second redox process of PBO interfering (Figure 3).

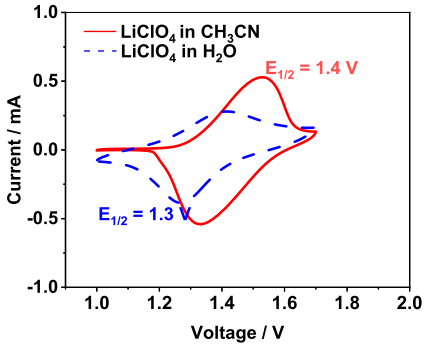

Figure 3. Cyclic voltammetry curves of coin cells at a scan rate of 1 mV s^{-1} containing PBO/PTMAm (blue) and PBO/PTMA (red) with 1 M $LiClO_4/H_2O$ and $LiClO_4/CH_3CN$ supporting electrolytes, respectively. Associated half-wave potentials are 1.3 and 1.4 V, respectively.

2.4. Battery Testing and Cycling Performance. *2.4.1. Screening of Different Electrolyte Systems.* In order to understand the behavior of PBO in the battery systems, the PBO electrodes were investigated in combination with oversized cathodes. Various electrolyte systems commonly employed in organic batteries were screened. The investigated electrolyte compositions are stated in Table 2. For this screening, the calculations on capacity utilization were performed without considering the counterion of the electrolyte. Following this initial screening (rate capability tests of **P1-PBO** vs TEMPO derivatives can be found in the Supporting

https://doi.org/10.1021/acsaem.4c03127
ACS Appl. Energy Mater. 2025, 8, 4220−4230

Table 2. Screening of Different Electrolyte Systems Commonly Employed in Organic Batteries

organic-based electrolytes	1 M $CH_3CN/TBAPF_6$	1 M $CH_3CN/TBAClO_4$	1 M $CH_3CN/LiClO_4$	1 M EC:DMC 3:7 $LiClO_4$	1 M TEGDME/$LiClO_4$	1 M $Pyr_{1,4}TFSI/PC$
aqueous-based electrolytes	2 M H_2O/LiOTf		1 M $H_2O/LiClO_4$		2 M H_2O/NaOTf	

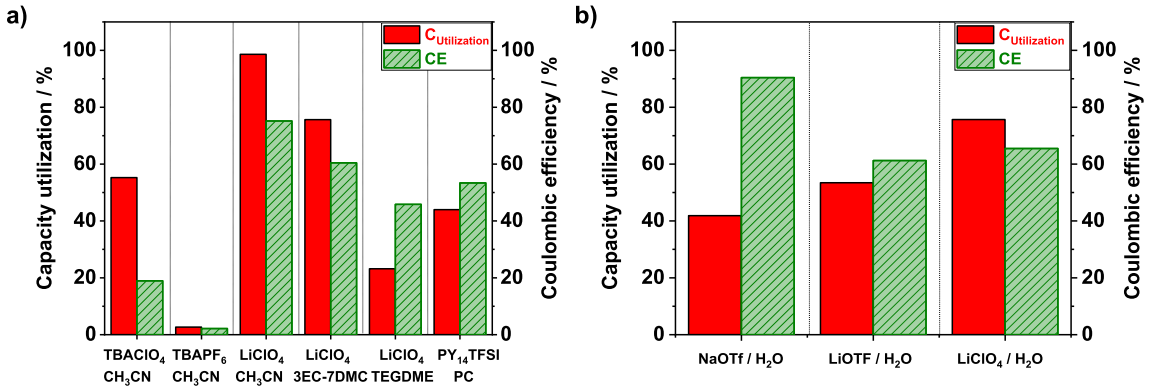

Figure 4. Dependence of the electrolyte on the initial (discharge) capacity utilization and the initial Coulombic efficiency (CE) in coin cell battery testing experiments. Calculations were performed using discharge capacities per electrode obtained at 1 C (first cycle). (a) Organic-based electrolytes and (b) aqueous-based electrolytes. Each bar represents the data from coin cells cycled under equal conditions.

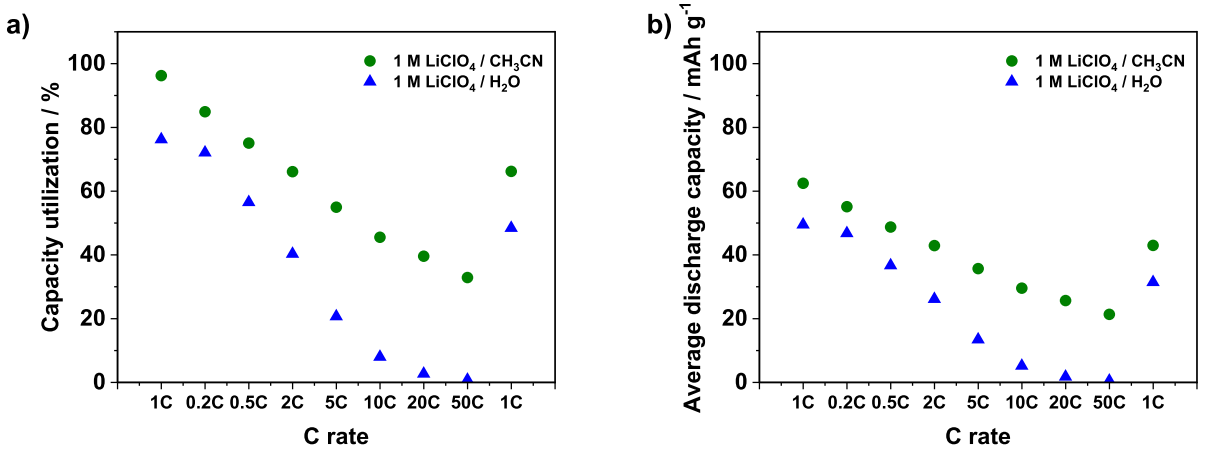

Figure 5. (a) Average capacity utilization (six cycles per C-rate) for **P1-PBO**/PTMA (green), using $LiClO_4/CH_3CN$, and **P1-PBO**/PTMAm (blue), using $LiClO_4/H_2O$ as the supporting electrolyte. (b) Average discharge capacity per C-rate for **P1-PBO**/PTMA (green) and **P1-PBO**/PTMAm (blue) batteries in organic- and aqueous-based electrolytes.

Information, Figures S16 and S17), the most promising system from both aqueous and organic electrolytes was selected for further in-depth investigations.

Out of six organic and three aqueous electrolyte systems, 1 M $LiClO_4$ in CH_3CN and 1 M $LiClO_4$ in H_2O provided a capacity utilization of >98% and >75% as well as an initial Coulombic efficiency of 75% and 65% at 1 C rate, respectively (Figure 4).

2.4.2. All-Organic Battery Performance. In both organic and aqueous electrolytes, the batteries exhibited a charging/discharging plateau between 1.2 and 1.5 V (selected charge/discharge curves can be found in the Supporting Information, Figures S26–S28).

In the battery system using $LiClO_4/CH_3CN$ as the electrolyte, due to a higher concentration of ClO_4^- ions coming from the electrolyte system in comparison to the Cl^- ions from PBO, an ion exchange within the system is expected to occur. This leads to a lower theoretically specific capacity for **P1-PBO** of 64.9 mA h g^{-1} (for PBO-ClO_4^-) instead of 76.8 mA h g^{-1} (for PBO-Cl^-). In what follows, all of the stated capacities are based on PBO-ClO_4^- and expressed per polymer mass. Experimentally, a value of 64 mA h g^{-1} was observed. This corresponds to a capacity utilization of 99% at 1 C in the first cycle. During the rate capability test, **P1-PBO** demonstrated capacity retention at both low and high C-rates. In particular, 59.9 mA h g^{-1} of the specific discharge capacity, giving 92% of capacity utilization, was observed at 0.2 C (cycle 1) and 21.3 mA h g^{-1} (33% of capacity utilization) at 50 C (cycle 1) (Figure 5a). After the capability rate test ended, the same cell was galvanostatically cycled at 1 C for 50 more cycles, leading to a final specific discharge capacity of 43.8 mA h g^{-1} (cycle 1), which corresponds to 68% capacity retention compared to the initial capacity. Only 47% of the capacity is retained after 100 cycles in total (Figure 6a).

During long-term experiments at 1 C with a new cell (Figure 6b), the composite electrode provided an initial specific discharge capacity of 57.8 mA h g^{-1}, which dropped to 37.5 mA h g^{-1} after 50 cycles, resulting in 65% capacity retention.

https://doi.org/10.1021/acsaem.4c03127
ACS Appl. Energy Mater. 2025, 8, 4220−4230

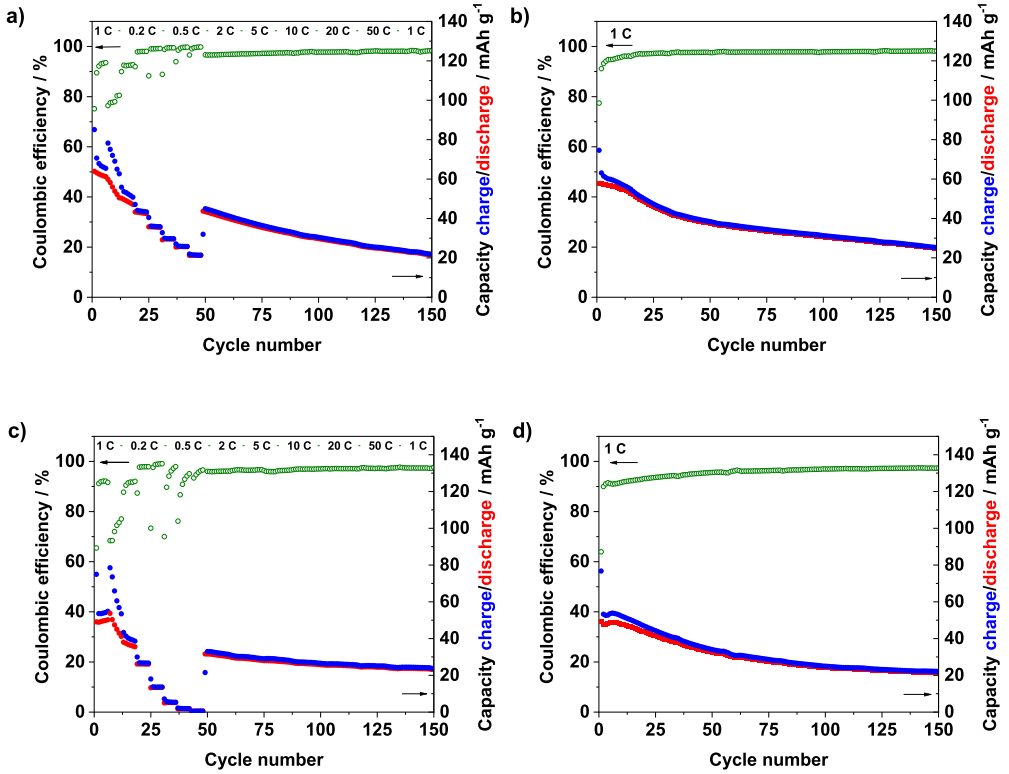

Figure 6. Coin cell experiments of **P1-PBO** vs TEMPO derivatives: (a,b) **P1-PBO**/PTMA battery in 1 M $LiClO_4$ in CH_3CN: (a) rate capability tests and (b) long-term experiments at 1 C and (c,d) **P1-PBO**/PTMAm battery in 1 M $LiClO_4$ in H_2O: (c) rate capability tests and (d) long-term experiments at 1 C.

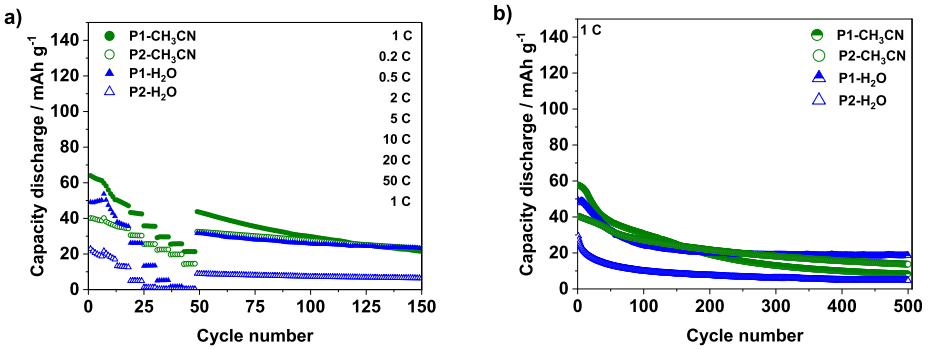

Figure 7. Comparison of battery performance of **P1-PBO** and **P2-PBO** polymers in aqueous- (1 M $LiClO_4/H_2O$): P1-H_2O, **P2-H_2O**, and organic-based (1 M $LiClO_4/CH_3CN$): P1-CH_3CN, **P2-CH_3CN**, electrolytes. (a) Rate capability test and (b) long-term experiments.

For the next 50 cycles, a further decay by 7 mA h g^{-1} was evident, indicating a slowdown in capacity decay, which is most likely connected to a saturation or a change in the decay mechanism. In the end, after 150 cycles, a specific discharge capacity of 24.8 mA h g^{-1} was observed. Overall, this corresponds to an average discharge capacity decay of about 0.7% per cycle (with a standard deviation of 0.3%) for the first 50 cycles and a decay of about 0.20% per cycle (with a standard deviation of 0.06%) for the last 100 cycles. The capacity decay in percentage is calculated by dividing the capacity decay per cycle by the initial discharge capacity. During a visual post-mortem inspection of the investigated coin cell components, it was noticed that the separator had a brown color (photographs of the cell separator can be found in the Supporting Information, Figure S29). Considering the linear nature of the PBO macromolecules, this observation implies the dissolution of **P1-PBO** in the electrolyte, which is likely the primary cause of capacity decay. The observed slowdown of the decay rate is most likely due to a saturation process of the molecule in the electrolyte or side reactions occurring while cycling.

The application of **P1-PBO** vs PTMAm in the 1 M $LiClO_4/H_2O$ electrolyte results in an initial discharge capacity of 49 mA h g^{-1} at 1 C, which corresponds to 76% of capacity utilization. During the rate capability test, a very low capacity was observed during fast discharge rates of 20 and 50 C (Figure 5b). Subsequent to the rate capability experiment, the cell was galvanostatically cycled at 1 C for 50 cycles, leading to a final specific discharge capacity of 31.7 mA h g^{-1}, which corresponds to 65% capacity retention compared to the initial discharge capacity. Furthermore, only 53% of the capacity is retained after 100 cycles (Figure 6c). Separate long-term experiments with pristine **P1-PBO** vs PTMAm batteries resulted in an initial specific discharge capacity of 49.1 mA h

https://doi.org/10.1021/acsaem.4c03127
ACS Appl. Energy Mater. 2025, 8, 4220−4230

g^{-1} (76% of capacity utilization), which further decayed to 32.5 mA h g^{-1} (66% capacity retention) after 50 cycles in agreement with the previous results. After 150 cycles, the battery reached a specific capacity of 21.6 mA h g^{-1} (44% of capacity retention) compared to the initial specific discharge capacity (Figure 6d). The presented results suggest that the capacity utilization is significantly higher in organic electrolyte systems compared to the investigated aqueous system. We assume that this is attributed to a different interaction of the active material with aqueous- and organic-based electrolytes, respectively, affecting the ability to deliver counterions to the active site. Additionally, the dissolution of the active material in an aqueous-based electrolyte is higher than in an organic-based electrolyte, causing a higher capacity decay over time.

While it was expected that a linear redox-active polymer would dissolve,[16,50] the same battery experiment tests were performed using the higher molar mass polymer **P2-PBO** as anode material vs TEMPO derivatives (**P2-PBO** vs PTMA using $LiClO_4/CH_3CN$ and **P2-PBO** vs PTMAm using $LiClO_4/H_2O$ as an electrolyte) (battery performance of **P2-PBO** vs TEMPO derivatives can be found in Supporting Information, Figures S22 and S23). The overall battery behavior of the **P2-PBO** anode in organic- and aqueous-based electrolytes was similar to **P1-PBO** anode battery performance (Figure 7). In both systems, the specific discharge capacity was decaying with the cycle number, but **P1-PBO** exhibited a 37% higher capacity utilization compared to **P2-PBO**. On the other hand, the **P2-PBO** anode exhibits a 13% higher capacity retention and, thus, a longer cycle life at 1 C (detailed battery performance of **P1-PBO** and **P2-PBO** can be found in Supporting Information, Figures S24 and S25), indicating a lower overall solubility. During the rate capability test, the experimentally observed discharge capacity for **P2-PBO** at 1 C (cycle 1) was 40.2 mA h g^{-1}. This corresponds to a capacity utilization of 62%. After the cyclability rate test ended, the same cell was galvanostatically cycled at 1 C for another 100 cycles, resulting in a discharge capacity of 23 mA h g^{-1} and 57% capacity retention compared to the initial capacity after 150 cycles in total (Figure 7a, **P2-CH_3CN**). During additional long-term experiments at 1 C, an initial experimental discharge capacity of 39.9 mA h g^{-1} was obtained, with a capacity decay of 0.4% per cycle (standard deviation of 0.2%) for the first 50 cycles to 0.1% (standard deviation 0.08%) after 450 cycles (Figure 7b, **P2-CH_3CN**). The application of 1 M $LiClO_4/H_2O$ electrolyte resulted in 35% capacity utilization at 1 C (cycle 1). At the end of rate capability tests, only 40% capacity is retained compared to the initial experimental capacity at 1 C (Figure 7a, **P2-H_2O**) (see Supporting Information, Figures S22 and S23 for details on rate capability tests and long-term experiments).

As expected, the obtained results indicate that a higher molar mass polymer leads to a slower dissolution of the material into the electrolyte and, thus, slower capacity decay per cycle (Figure 7b) (selected cycles of voltage vs time curves can be found in Supporting Information, Figures S27 and S28). Additionally, the lower capacity utilization of **P2-PBO** compared to **P1-PBO** is due to the difficult interaction between the higher molar mass polymer and the electrolyte.

3. CONCLUSIONS

In this study, we introduced a new class of redox polymers for organic thin-film batteries, which is based on the benzo-oxazole molecule. With poly(4-(benzo[*d*]oxazol-2-yl)-1-(4-(*sec*-butyl)-benzyl)pyridin-1-ium chloride) (PBO), a first representative of this class was synthesized and investigated as anode material in all-organic batteries. A molecule has a theoretical specific capacity of 76.8 mA h g^{-1} (first redox process).

Linear PBO was obtained from a comparably straightforward synthetic procedure in two batches with relatively small molar masses of 3500 g mol^{-1} (**P1-PBO**) and 5100 g mol^{-1} (**P2-PBO**), respectively. The DFT calculations of the BO monomer and PBO model systems have provided deeper insight into the redox reactions as well as the spin and charge distribution of the monomer and polymer. The results suggest that the PBO possesses an oxidation and reduction potential comparable to or slightly lower than those of the BO monomer.

Experimental half-wave potentials of the BO monomer and PBO were obtained by performing cycling voltammetry measurements in 0.1 M $TBAPF_6$ in CH_3CN, where the experimental redox processes observed correlate with the presented theoretical calculations. Due to stability issues of the second redox process, only the first redox process was used for battery investigations. Both **P1-PBO** and **P2-PBO** were applied as anode materials in two types of coin cells utilizing either a PTMA cathode and 1 M $LiClO_4$ in CH_3CN or a PTMAm cathode and 1 M $LiClO_4$ in H_2O. Due to the higher concentration of ClO_4^- ions in the battery cell, an ion exchange from Cl^- to ClO_4^- can be expected to take place, resulting in a theoretical specific capacity of 64.9 mA h g^{-1}. The batteries with the organic electrolyte revealed a capacity utilization of more than 90% at 1 C and a capacity decay of about 0.7% per cycle (standard deviation of 0.3%) for the first 50 cycles. In addition, the increase of the molar mass of the polymer **P2-PBO** not only lowered the capacity utilization but also slightly slowed down the capacity decay to 0.4% (standard deviation of 0.2%) over the same number of cycles. Additionally, during long-term experiments at 1 C, **P2-PBO** exhibits a longer lifetime stability compared to **P1-PBO**. On the other hand, the aqueous battery exhibited a significantly lower capacity utilization of 76% for **P1-PBO** and 35% for **P2-PBO**, respectively. In either case, the significant capacity loss is attributed to the dissolution of the linear polymer into the electrolyte, as supported by visual post-mortem analysis. This issue will be addressed by upcoming studies, which will investigate the cross-linking of PBO and possibly other mitigation strategies. The latter could involve the optimization of the electrolyte properties, such as using solvent-free electrolytes or gel-polymer electrolytes. Despite the remaining performance issues, the obtained results are promising for this novel class of redox polymers for organic thin-film batteries.

This work will initiate further research on benzoxazole-based electrode materials for organic-based batteries. Our ongoing research focuses on reducing the polymers' solubility and understanding the battery degradation mechanisms.

■ ASSOCIATED CONTENT

Supporting Information

The Supporting Information is available free of charge at https://pubs.acs.org/doi/10.1021/acsaem.4c03127.

Materials and methods; HPLC, AUC, and additional theoretical results; and battery performance results (PDF)

https://doi.org/10.1021/acsaem.4c03127
ACS Appl. Energy Mater. 2025, 8, 4220−4230

AUTHOR INFORMATION

Corresponding Author

Ulrich S. Schubert − *Laboratory of Organic and Macromolecular Chemistry (IOMC), Friedrich Schiller University Jena, 07743 Jena, Germany; Center for Energy and Environmental Chemistry Jena (CEEC Jena), Friedrich Schiller University Jena, 07743 Jena, Germany; Helmholtz Institute for Polymers in Energy Applications Jena (HIPOLE Jena), 07743 Jena, Germany; Helmholtz-Zentrum Berlin für Materialien und Energie GmbH (HZB), 14109 Berlin, Germany;* orcid.org/0000-0003-4978-4670; Email: ulrich.schubert@uni-jena.de

Authors

Xhesilda Fataj − *Laboratory of Organic and Macromolecular Chemistry (IOMC), Friedrich Schiller University Jena, 07743 Jena, Germany; Center for Energy and Environmental Chemistry Jena (CEEC Jena), Friedrich Schiller University Jena, 07743 Jena, Germany*

Andreas J. Achazi − *Center for Materials Research Justus-Liebig University Giessen, 35392 Giessen, Germany; Institute of Physical Chemistry Justus-Liebig University Giessen, 35392 Giessen, Germany;* orcid.org/0000-0002-3001-875X

Christian Stolze − *Laboratory of Organic and Macromolecular Chemistry (IOMC), Friedrich Schiller University Jena, 07743 Jena, Germany; Center for Energy and Environmental Chemistry Jena (CEEC Jena), Friedrich Schiller University Jena, 07743 Jena, Germany;* orcid.org/0000-0001-5358-7181

Simon Muench − *Laboratory of Organic and Macromolecular Chemistry (IOMC), Friedrich Schiller University Jena, 07743 Jena, Germany; Center for Energy and Environmental Chemistry Jena (CEEC Jena), Friedrich Schiller University Jena, 07743 Jena, Germany;* orcid.org/0000-0003-3710-4682

René Burges − *Laboratory of Organic and Macromolecular Chemistry (IOMC), Friedrich Schiller University Jena, 07743 Jena, Germany; Center for Energy and Environmental Chemistry Jena (CEEC Jena), Friedrich Schiller University Jena, 07743 Jena, Germany*

Ilya Anufriev − *Laboratory of Organic and Macromolecular Chemistry (IOMC), Friedrich Schiller University Jena, 07743 Jena, Germany; Center for Energy and Environmental Chemistry Jena (CEEC Jena), Friedrich Schiller University Jena, 07743 Jena, Germany; Helmholtz Institute for Polymers in Energy Applications Jena (HIPOLE Jena), 07743 Jena, Germany*

Manon Mignon − *Faculté des Sciences, Université de Montpellier, 34095 Montpellier Cedex 5, France*

Doreen Mollenhauer − *Center for Materials Research Justus-Liebig University Giessen, 35392 Giessen, Germany; Institute of Physical Chemistry Justus-Liebig University Giessen, 35392 Giessen, Germany; Helmholtz Institute for Polymers in Energy Applications Jena (HIPOLE Jena), 07743 Jena, Germany; Institute for Technical and Environmental Chemistry, Friedrich Schiller University Jena, 07743 Jena, Germany; Helmholtz-Zentrum Berlin für Materialien und Energie GmbH (HZB), 14109 Berlin, Germany;* orcid.org/0000-0003-0084-4599

Ivo Nischang − *Laboratory of Organic and Macromolecular Chemistry (IOMC), Friedrich Schiller University Jena, 07743 Jena, Germany; Center for Energy and Environmental Chemistry Jena (CEEC Jena), Friedrich Schiller University Jena, 07743 Jena, Germany; Helmholtz Institute for Polymers in Energy Applications Jena (HIPOLE Jena), 07743 Jena, Germany; Helmholtz-Zentrum Berlin für Materialien und Energie GmbH (HZB), 14109 Berlin, Germany;* orcid.org/0000-0001-6182-5215

Martin D. Hager − *Laboratory of Organic and Macromolecular Chemistry (IOMC), Friedrich Schiller University Jena, 07743 Jena, Germany; Center for Energy and Environmental Chemistry Jena (CEEC Jena), Friedrich Schiller University Jena, 07743 Jena, Germany; Helmholtz Institute for Polymers in Energy Applications Jena (HIPOLE Jena), 07743 Jena, Germany;* orcid.org/0000-0002-6373-6600

Complete contact information is available at: https://pubs.acs.org/10.1021/acsaem.4c03127

Author Contributions

The manuscript was written through contributions of all authors. All authors have given approval to the final version of the manuscript.

Notes

The authors declare no competing financial interest.

ACKNOWLEDGMENTS

The authors would like to thank the Deutsche Forschungsgemeinschaft (DFG), in particular the priority program "Polymer-based Batteries" (SPP 2248, project number 441217366). We would also like to thank the Université de Montpellier for realizing the internship of M.M. The authors acknowledge computational resources provided by the HPC Core Facility and the HRZ of the Justus-Liebig-University Giessen. I.N. acknowledges funding by the DFG—471397362.

REFERENCES

(1) Kim, J.; Kim, Y.; Yoo, J.; Kwon, G.; Ko, Y.; Kang, K. Organic batteries for a greener rechargeable world. *Nat. Rev. Mater.* **2023**, *8* (1), 54−70.

(2) Goujon, N.; Casado, N.; Patil, N.; Marcilla, R.; Mecerreyes, D. Organic batteries based on just redox polymers. *Prog. Polym. Sci.* **2021**, *122*, 101449.

(3) Janoschka, T.; Hager, M. D.; Schubert, U. S. Powering up the Future: Radical Polymers for Battery Applications. *Adv. Mater.* **2012**, *24* (48), 6397−6409.

(4) Lin, Z.; Shi, H.-Y.; Lin, L.; Yang, X.; Wu, W.; Sun, X. A high capacity small molecule quinone cathode for rechargeable aqueous zinc-organic batteries. *Nat. Commun.* **2021**, *12* (1), 4424.

(5) Hendriks, K. H.; Sevov, C. S.; Cook, M. E.; Sanford, M. S. Multielectron Cycling of a Low-Potential Anolyte in Alkali Metal Electrolytes for Nonaqueous Redox Flow Batteries. *ACS Energy Lett.* **2017**, *2* (10), 2430−2435.

(6) Nishide, H.; Iwasa, S.; Pu, Y.-J.; Suga, T.; Nakahara, K.; Satoh, M. Organic radical battery: nitroxide polymers as a cathode-active material. *Electrochim. Acta* **2004**, *50*, 827−831.

(7) Schröter, E.; Elbinger, L.; Mignon, M.; Friebe, C.; Brendel, J. C.; Hager, M. D.; Schubert, U. S. High-capacity semi-organic polymer batteries: From monomer to battery in an all-aqueous process. *J. Power Sources* **2023**, *556*, 232293.

(8) Bugnon, L.; Morton, C. J. H.; Novak, P.; Vetter, J.; Nesvadba, P. Synthesis of Poly(4-methacryloyloxy-TEMPO) via Group-Transfer Polymerization and Its Evaluation in Organic Radical Battery. *Chem. Mater.* **2007**, *19* (11), 2910−2914.

(9) Hong, Y.; Hu, J.; Tang, W.; Wei, B.; Guo, M.; Jia, S.; Fan, C. A universal small-molecule organic cathode for high-performance Li/Na/K-ion batteries. *Energy Storage Mater.* **2022**, *52*, 61−68.

(10) Wang, X.; Tang, W.; Hu, Y.; Liu, W.; Yan, Y.; Xu, L.; Fan, C. Insoluble small-molecule organic cathodes for highly efficient pure-organic Li-ion batteries. *Green Chem.* **2021**, *23* (16), 6090−6100.
(11) Saal, A.; Elbinger, L.; Schreyer, K.; Fataj, X.; Friebe, C.; Schubert, U. S. Structural Improvement of the Blatter Radical for High-Current Organic Batteries. *ACS Appl. Energy Mater.* **2022**, *5* (12), 15019−15028.
(12) Zhu, L. M.; Lei, A. W.; Cao, Y. L.; Ai, X. P.; Yang, H. X. An all-organic rechargeable battery using bipolar polyparaphenylene as a redox-active cathode and anode. *Chem. Commun.* **2013**, *49* (6), 567−569.
(13) Dong, X.; Yu, H.; Ma, Y.; Bao, J. L.; Truhlar, D. G.; Wang, Y.; Xia, Y. All-Organic Rechargeable Battery with Reversibility Supported by "Water-in-Salt" Electrolyte. *Chem.—Eur. J.* **2017**, *23* (11), 2560−2565.
(14) Poizot, P.; Gaubicher, J.; Renault, S.; Dubois, L.; Liang, Y.; Yao, Y. Opportunities and Challenges for Organic Electrodes in Electrochemical Energy Storage. *Chem. Rev.* **2020**, *120* (14), 6490−6557.
(15) Nakahara, K.; Iwasa, S.; Satoh, M.; Morioka, Y.; Iriyama, J.; Suguro, M.; Hasegawa, E. Rechargeable batteries with organic radical cathodes. *Chem. Phys. Lett.* **2002**, *359* (5), 351−354.
(16) Muench, S.; Gerlach, P.; Burges, R.; Strumpf, M.; Hoeppener, S.; Wild, A.; Lex-Balducci, A.; Balducci, A.; Brendel, J. C.; Schubert, U. S. Emulsion Polymerizations for a Sustainable Preparation of Efficient TEMPO-based Electrodes. *ChemSusChem* **2021**, *14* (1), 449−455.
(17) Kim, J.-K.; Cheruvally, G.; Ahn, J.-H.; Seo, Y.-G.; Choi, D. S.; Lee, S.-H.; Song, C. E. Organic radical battery with PTMA cathode: Effect of PTMA content on electrochemical properties. *J. Ind. Eng. Chem.* **2008**, *14* (3), 371−376.
(18) Kolek, M.; Otteny, F.; Schmidt, P.; Mück-Lichtenfeld, C.; Einholz, C.; Becking, J.; Schleicher, E.; Winter, M.; Bieker, P.; Esser, B. Ultra-high cycling stability of poly(vinylphenothiazine) as a battery cathode material resulting from $\pi-\pi$ interactions. *Energy Environ. Sci.* **2017**, *10* (11), 2334−2341.
(19) Song, Z.; Qian, Y.; Zhang, T.; Otani, M.; Zhou, H. Poly(benzoquinonyl sulfide) as a High-Energy Organic Cathode for Rechargeable Li and Na Batteries. *Adv. Sci.* **2015**, *2* (9), 1500124.
(20) Sevov, C. S.; Hendriks, K. H.; Sanford, M. S. Low-Potential Pyridinium Anolyte for Aqueous Redox Flow Batteries. *J. Phys. Chem. C* **2017**, *121* (44), 24376−24380.
(21) Striepe, L.; Baumgartner, T. Viologens and Their Application as Functional Materials. *Chem.—Eur. J.* **2017**, *23* (67), 16924−16940.
(22) Luo, J.; Hu, B.; Debruler, C.; Liu, T. L. A π-Conjugation Extended Viologen as a Two-Electron Storage Anolyte for Total Organic Aqueous Redox Flow Batteries. *Angew. Chem., Int. Ed.* **2018**, *57* (1), 231−235.
(23) Sano, N.; Tomita, W.; Hara, S.; Min, C.-M.; Lee, J.-S.; Oyaizu, K.; Nishide, H. Polyviologen Hydrogel with High-Rate Capability for Anodes toward an Aqueous Electrolyte-Type and Organic-Based Rechargeable Device. *ACS Appl. Mater. Interfaces* **2013**, *5* (4), 1355−1361.
(24) Fataj, X.; Achazi, A. J.; Rohland, P.; Schröter, E.; Muench, S.; Burges, R.; Pohl, K. L. H.; Mollenhauer, D.; Hager, M. D.; Schubert, U. S. Development of Novel Redox-Active Organic Materials Based on Benzimidazole, Benzoxazole, and Benzothiazole: A Combined Theoretical and Experimental Screening Approach. *Chem.—Eur. J.* **2023**, *30*, No. e202302979.
(25) Sen, S.; Saraidaridis, J.; Kim, S. Y.; Palmore, G. T. R. Viologens as Charge Carriers in a Polymer-Based Battery Anode. *ACS Appl. Mater. Interfaces* **2013**, *5* (16), 7825−7830.
(26) Achazi, A. J.; Fataj, X.; Rohland, P.; Hager, M. D.; Schubert, U. S.; Mollenhauer, D. Development of a multi-step screening procedure for redox active molecules in organic radical polymer anodes and as redox flow anolytes. *J. Comput. Chem.* **2024**, *45* (14), 1112−1129.
(27) Fornari, R. P.; de Silva, P. Molecular modeling of organic redox-active battery materials. *Wiley Interdiscip. Rev.: Comput. Mol. Sci.* **2021**, *11* (2), No. e1495.
(28) Er, S.; Suh, C.; Marshak, M. P.; Aspuru-Guzik, A. Computational design of molecules for an all-quinone redox flow battery. *Chem. Sci.* **2015**, *6* (2), 885−893.
(29) Zaichenko, A.; Achazi, A. J.; Kunz, S.; Wegner, H. A.; Janek, J.; Mollenhauer, D. Static theoretical investigations of organic redox active materials for redox flow batteries. *Prog. Energy* **2024**, *6* (1), 012001.
(30) Hager, M. D.; Esser, B.; Feng, X.; Schuhmann, W.; Theato, P.; Schubert, U. S. Polymer-Based Batteries—Flexible and Thin Energy Storage Systems. *Adv. Mater.* **2020**, *32* (39), 2000587.
(31) Gerlach, P.; Balducci, A. A Critical Analysis about the Underestimated Role of the Electrolyte in Batteries Based on Organic Materials. *ChemElectroChem* **2020**, *7* (11), 2364−2375.
(32) Wessling, R.; Koger, H.; Otteny, F.; Schmidt, M.; Semmelmaier, A.; Esser, B. Unlocking twofold oxidation in phenothiazine polymers for application in symmetric all-organic anionic batteries. *ACS Appl. Polym. Mater.* **2024**, *6* (14), 7956−7968.
(33) Jouhara, A.; Quarez, E.; Dolhem, F.; Armand, M.; Dupré, N.; Poizot, P. Tuning the Chemistry of Organonitrogen Compounds for Promoting All-Organic Anionic Rechargeable Batteries. *Angew. Chem.* **2019**, *131* (44), 15827−15831.
(34) Bhosale, M.; Schmidt, C.; Penert, P.; Studer, G.; Esser, B. Anion-Rocking Chair Batteries with Tuneable Voltage using Viologen- and Phenothiazine Polymer-based Electrodes. *ChemSusChem* **2024**, *17* (5), No. e202301143.
(35) Liu, Q.; Wang, Y.; Yang, X.; Zhou, D.; Wang, X.; Jaumaux, P.; Kang, F.; Li, B.; Ji, X.; Wang, G. Rechargeable anion-shuttle batteries for low-cost energy storage. *Chem* **2021**, *7* (8), 1993−2021.
(36) Uhl, M.; Penert, P.; Penert, P.; Schuster, P. A.; Schick, B. W.; Muench, S.; Farkas, A.; Schubert, U. S.; Esser, B.; Kuehne, A. J. C.; et al. All-Organic Battery Based on Deep Eutectic Solvent and Redox-Active Polymers. *ChemSusChem* **2024**, *17* (1), No. e202301057.
(37) Brown, P. H.; Schuck, P. Macromolecular Size-and-Shape Distributions by Sedimentation Velocity Analytical Ultracentrifugation. *Biophys. J.* **2006**, *90* (12), 4651−4661.
(38) Grube, M.; Dinu, V.; Lindemann, H.; Pielenz, F.; Festag, G.; Schubert, U. S.; Heinze, T.; Harding, S.; Nischang, I. Polysaccharide valproates: Structure - property relationships in solution. *Carbohydr. Polym.* **2020**, *246*, 116652.
(39) Dirac, P. A. M. Quantum mechanics of many-electron systems. *Proc. R. Soc. London, Ser. A* **1929**, *123* (792), 714−733.
(40) Slater, J. C. A simplification of the Hartree-Fock method. *Phys. Rev.* **1951**, *81* (3), 385.
(41) Vosko, S. H.; Wilk, L.; Nusair, M. Accurate spin-dependent electron liquid correlation energies for local spin density calculations: a critical analysis. *Can. J. Phys.* **1980**, *58* (8), 1200−1211.
(42) Becke, A. D. Density-functional exchange-energy approximation with correct asymptotic behavior. *Phys. Rev. A:At., Mol., Opt. Phys.* **1988**, *38* (6), 3098.
(43) Lee, C.; Yang, W.; Parr, R. G. Development of the Colle-Salvetti correlation-energy formula into a functional of the electron density. *Phys. Rev. B:Condens. Matter Mater. Phys.* **1988**, *37* (2), 785.
(44) Becke, A. D. Density-functional thermochemistry. III. The role of exact exchange. *J. Chem. Phys.* **1993**, *98* (7), 5648−5652.
(45) Caldeweyher, E.; Bannwarth, C.; Grimme, S. Extension of the D3 dispersion coefficient model. *J. Chem. Phys.* **2017**, *147* (3), 034112.
(46) Caldeweyher, E.; Ehlert, S.; Hansen, A.; Neugebauer, H.; Spicher, S.; Bannwarth, C.; Grimme, S. A generally applicable atomic-charge dependent London dispersion correction. *J. Chem. Phys.* **2019**, *150* (15), 154122.
(47) Weigend, F.; Ahlrichs, R. Balanced basis sets of split valence, triple zeta valence and quadruple zeta valence quality for H to Rn: Design and assessment of accuracy. *Phys. Chem. Chem. Phys.* **2005**, *7* (18), 3297−3305.
(48) Weigend, F. Accurate Coulomb-fitting basis sets for H to Rn. *Phys. Chem. Chem. Phys.* **2006**, *8* (9), 1057−1065.
(49) Schröter, E.; Stolze, C.; Meyer, J.; Hager, M. D.; Schubert, U. S. Organic Redox Targeting Flow Battery Utilizing a Hydrophilic

Polymer and Its In-Operando Characterization via State-of-Charge Monitoring of The Redox Mediator. *ChemSusChem* **2023**, *16* (14), No. e202300296.

(50) Acker, P.; Speer, M. E.; Wössner, J. S.; Esser, B. Azine-based polymers with a two-electron redox process as cathode materials for organic batteries. *J. Mater. Chem. A* **2020**, *8* (22), 11195−11201.

https://doi.org/10.1021/acsaem.4c03127
ACS Appl. Energy Mater. 2025, 8, 4220−4230